J Mater Sci: Mater Electron (2024) 35:385

Photoluminescence enhancement of chemical vapor-deposited $MoSe_2$ monolayers

A. S. Kopar[1,2], A. Coşkun[2,3], M. A. Çağlar[2,3,4], M. Ertuğrul[5,6], and Güven Turgut[2,3,4,*]

[1] *Department of Electric and Electronic Engineering, Engineering Faculty, Atatürk University, 25240 Erzurum, Turkey*
[2] *2D Material Research Lab, High Technology Research and Application Centre, Erzurum Technical University, 25100 Erzurum, Turkey*
[3] *Department of Photonics, Science Institute, Erzurum Technical University, 25100 Erzurum, Turkey*
[4] *Department of Basic Sciences, Science Faculty, Erzurum Technical University, 25100 Erzurum, Turkey*
[5] *Department of Metallurgical and Materials Engineering, Engineering Faculty, Karadeniz Technical University, 61080 Trabzon, Turkey*
[6] *Institute of Nanoscience&Nanotechnology (ION2), Universiti Putra Malaysia, UPM, 43400 Serdang, Selangor, Malaysia*

Received: 16 November 2023
Accepted: 4 February 2024

© The Author(s), 2024

ABSTRACT

The transition metal dichalcogenide (TMDC) materials have attracted a great interest owing to their superior features. The chemical vapor deposition (CVD) is very feasible to synthesis of TMDC materials. The thermal expansion coefficient difference between TMDC materials and substrate in the CVD synthesis can cause a strain, resulting in non-radiative recombination and PL decrement for these materials. Therefore, in this work, we studied acetone and isopropanol (IPA) treatment on the photoluminescence (PL) properties of CVD-grown $MoSe_2$ monolayers. Firstly, monolayer $MoSe_2$ flakes on SiO_2/Si substrates were synthesized via the CVD method by optimizing synthesis parameters. The Raman and PL measurements were taken after acetone and IPA treatments were applied to grown samples. The results indicated an important PL enhancement was seen for acetone treatment. For IPA treatment, there was a PL peak position shifting with decreasing intensity due to its possible structural damage. The acetone, IPA, and transfer processes caused the releasing strain on $MoSe_2$ by breaking the strong interaction between $MoSe_2$ and substrate. For the whole treatment, PL peaks shift to blue with about 80 meV. As a result of the present study, acetone treatment was found as an easy and quick way to enhance radiative emission of CVD-grown $MoSe_2$.

1 Introduction

For 15 years, graphene has gained a great interest among the materials community due to its fascinating properties [1]. The lack of an intrinsic band gap in the graphene has led to the design and development of new kind two-dimensional (2D) materials, such as black phosphorous, hexagonal boron nitride (h-BN), and transition metal dichalcogenides (TMDCs) with a formula of MX_2 (M = TMs, X = S, Se, Te). Transition metal dichalcogenides have been very significant in solar cells, field effect transistors (FETs), gas sensing,

Address correspondence to E-mail: guven.turgut@erzurum.edu.tr

https://doi.org/10.1007/s10854-024-12140-3
Published online: 23 February 2024

hydrogen evolution reactions (HERs), spintronics, valleytronics, optoelectronic, biomedical, biosensing, and energy storage applications because of their controllable band gap and excellent striking mechanical and electronic properties [2–6]. Among TMDCs, the semiconducting monolayer $MoSe_2$ exhibits a direct band gap with PL [7]. The tunable PL properties of $MoSe_2$ are based on the defects, strain, doping, and number of layers [8, 9]. The band gap of MoS_2, $MoSe_2$, WS_2, and WSe_2 decreases gradually with tensile strain and then a transition from direct to indirect occurs [10–12], resulting in a subsequent decrease in PL intensity [13].

TMDC monolayers have been generally synthesized via the chemical vapor deposition (CVD) technique due to its simple and cost-effective apparatus [14]. In the CVD growth of $MoSe_2$, high temperature is necessary to deposit monolayer [14]. The difference in thermal expansion coefficient between $MoSe_2$ and SiO_2/Si (or other substrates) substrates brings about an important mismatch and strain. The thermal expansion coefficient of SiO_2 is much smaller than $MoSe_2$ and it will be in the tensile strains after CVD growth [15]. In the literature, it has been observed that tensile strain caused a shift of PL peak position to red and an important decrease in the PL intensity [16], which limits the usage of $MoSe_2$ in photonic applications. In the studies conducted by Kim et al. [16] and Chen et al. [17], the strain was released by decoupling the WSe_2, MoS_2, and $MoSe_2$ monolayers and substrate with high vapor pressure solvents (acetone, ethanol, toluene, methyl acetate, IPA, etc.). Kim et al. [16] are pioneers for the solvent decoupling study and they found also an important PL enhancement and 80-meV blue shift in PL position with acetone, methanol, IPA, and ethanol treatments. In the second work [17], it was found that acetone treatment caused a small change in the PL intensity (especially decrease for $MoSe_2$) and observed the blue shifts in the PL positions to be 54 meV and 2.4 meV for $MoSe_2$ and MoS_2 monolayers, respectively. The ethanol was also found most effective PL enhancement solvents for CVD-grown MoS_2 and $MoSe_2$ monolayers. Apart from the research based on strain decoupling, Borodin et al. [18] showed the anodic oxidation of the $MoSe_2$ multilayer structure brought about three times enhancement in the PL intensity. Moreover, it was found that oleic acid (OA) treatment for $MoSe_2$ caused a significant 58-fold improvement in the efficiency of PL and a reduction in the emission line width owing to the passivation of the Mo dangling bonds, which are faults that arise during manufacture, by OA treatment [19]. Similarly, p-doping of hydrohalic acid treatment on $MoSe_2$ can suppress trap state emissions, reduce structural defects, and increase PL density by 30 times compared to its previous state due to allowing for neutral exciton and trion peaks instead of negative trions [20, 21]. As a result of the literature survey, in the present work, we first carried out growth of $MoSe_2$ monolayer with CVD and then conducted a systematic approach to see the strain effect on PL and Raman spectra by decoupling tensile strain on $MoSe_2$ monolayer with acetone and isopropyl alcohol (IPA). To our knowledge, this has been the first study based on an important PL enhancement and decrement with acetone and IPA by decoupling tensile strain on $MoSe_2$ monolayer, respectively.

2 Materials and methods

A simple CVD method was used to synthesize monolayer $MoSe_2$ layers on SiO_2/Si substrates using MoO_3 and Se powders to be Mo and Se precursors, respectively. At first, it optimized CVD parameters such as amount of precursor MoO_3 and H_2 gas flow rate. The temperatures of the CVD furnace center and the Se powder upstream were 780 °C and 300 °C, respectively. The optimized Ar and H_2 (Ar/H_2 = 45 sccm/5 sccm) were used as carrier gases. After 12-min growth, the furnace was opened and cooled naturally to the room temperature. After optimized synthesis of ML $MoSe_2$ flakes on SiO_2/Si substrates, we dropped acetone and IPA on the samples and recollected PL and Raman spectra 10 min later. The grown ML structures were first observed with an optical microscope (ZEISS Axio Scope A1). Raman and photoluminescence spectra were collected with the Witech Alpha 300R micro-Raman system by exciting with a 532-nm green laser. SEM image was taken with Quanta FEG 250 SEM. The layer thickness was determined to be 0.8 nm with Hitachi 5100 N AFM.

3 Results and discussion

The synthesis of $MoSe_2$ with different morphologies was achieved by gradually increasing the amount of MoO_3 powder from 2 mg to 4 mg. When 2-mg MoO_3 powder was used, it found etched triangular structures based on $MoSe_2$ (Fig. 1b). In addition,

the precursor powder was gradually increased, and the bulk and smooth-edged triangles were observed (Fig. 1c). However, when the amount of powder reached 4 mg, hexagons were observed instead of the triangular shapes (Fig. 1d). The samples synthesized using the amount of 3-mg MoO_3 precursor exhibited the best triangular form, despite bulk form, and better lateral size compared to the other amounts (Fig. 1c). After optimization of MoO_3 amount, hydrogen gas flow rate was changed from 1 sccm to 7 sccm with a constant flow rate of Ar. When the H_2 flow rate was used to be 1 sccm, the results demonstrated the presence of stars which intertwined triangular structures and small lateral size of triangular structures (Fig. 1e). However, as increasing it to 5 sccm (Fig. 1f), the edges of triangular became smooth and lateral size increased. The flow rate of 7 sccm caused quite small triangular (~ 1 μm) and multilateral morphologies (Fig. 1g). As a result, the experiments showed that precursor powder quantity and H_2 gas flow rate greatly influenced $MoSe_2$ morphology, and it indicated (Fig. 1f) that the best result was achieved with 3-mg MoO_3 precursor

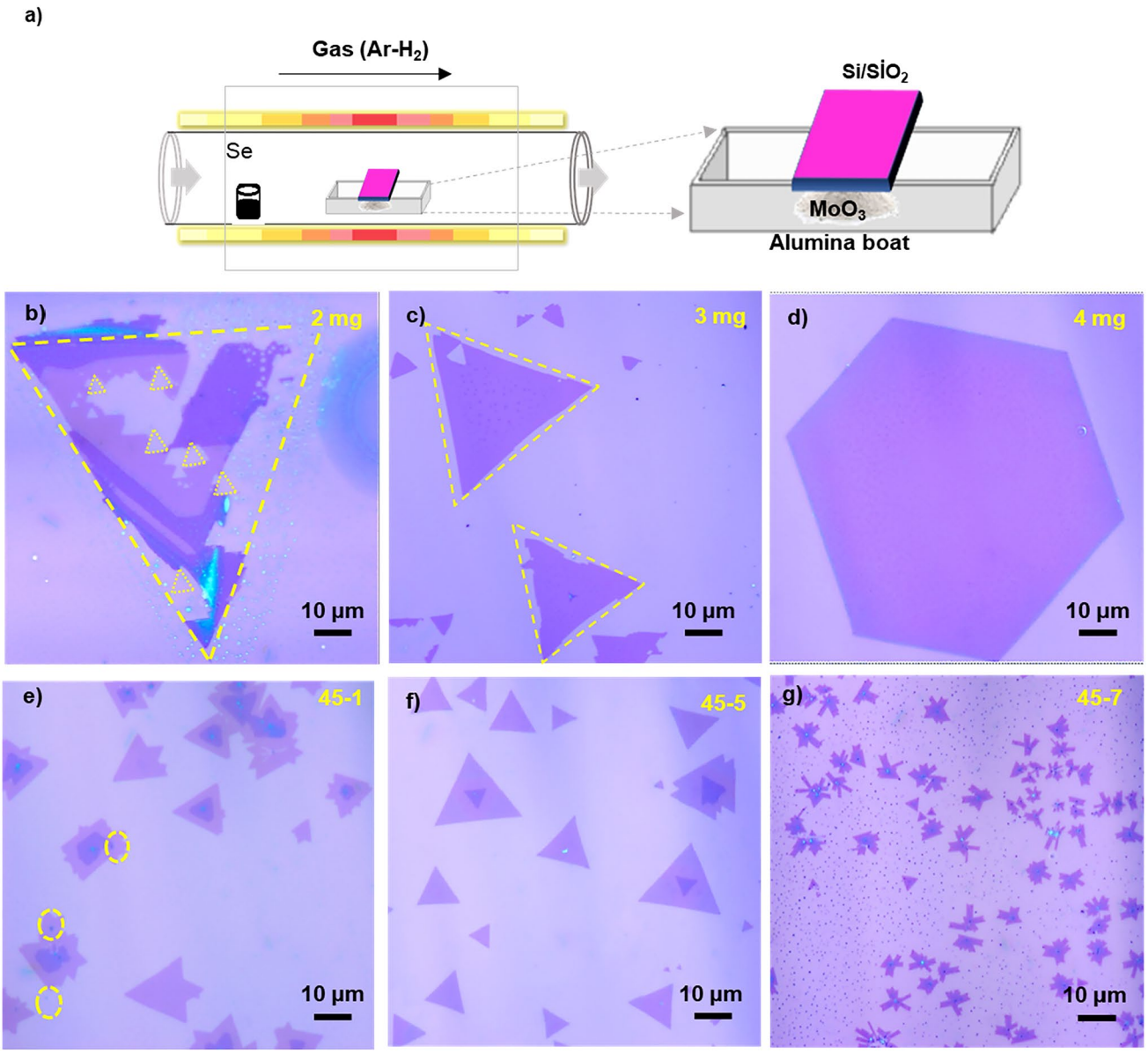

Fig. 1 **a** Schematic illustration of a CVD setup using MoO_3 and Se powder as the sources to create ultrathin $MoSe_2$ flakes on a Si/SiO_2 substrate. **b–e** Optical microscope images of MoSe2 monolayers grown depending on amount of MoO_3 and gas flow rate

amount and 45:5 sccm Ar:H_2 gas flow rate. The biggest lateral size of $MoSe_2$ MLs is about 200 μm^2 and the substrate is generally covered with monolayer flakes. In order to verify the crystal quality and composition of the samples as shown in Fig. 1f, it was characterized via Raman spectroscopy (Fig. 2a). Two characteristic Raman peaks for 2H $MoSe_2$ corresponding to A_{1g} (out-of-plane) and E_{2g} (in-plane) modes are observed at 243.7 cm^{-1} and 287.8 cm^{-1} [22], respectively (Fig. 2a). The sharp excitonic PL peak is located at 1.50 eV (Fig. 2b) that is related to direct transition of A exciton at the K-point of Brillouin zone, which is giving an optical band gap of $MoSe_2$ [22, 23]. The monolayer 2H $MoSe_2$ has normally two excitonic peaks of A and B because of valence band splitting at the K-point caused by the strong spin-orbit coupling (SOC) [24]. In this work, the excitonic B transition is not seen because of the low recombination of charge carriers [24]. The monolayer flakes are determined with AFM (see Fig. 2c) with 0.9 nm thickness. The SEM and EDX analyses presented in Fig. 2d indicated that Mo:Se atomic ratio is 1.00:2.05 which belongs to the defect-free $MoSe_2$ structure.

The synthesis of $MoSe_2$ layers during chemical vapor deposition (CVD) synthesis is attributed to the combination of evaporated MoO_3 and Se radicals on the substrate, resulting in the creation of Mo_xSe_{2-x} nuclei [25]. This emphasizes the significance of the quantity of precursors that were increased throughout the experiment. In this work, as the

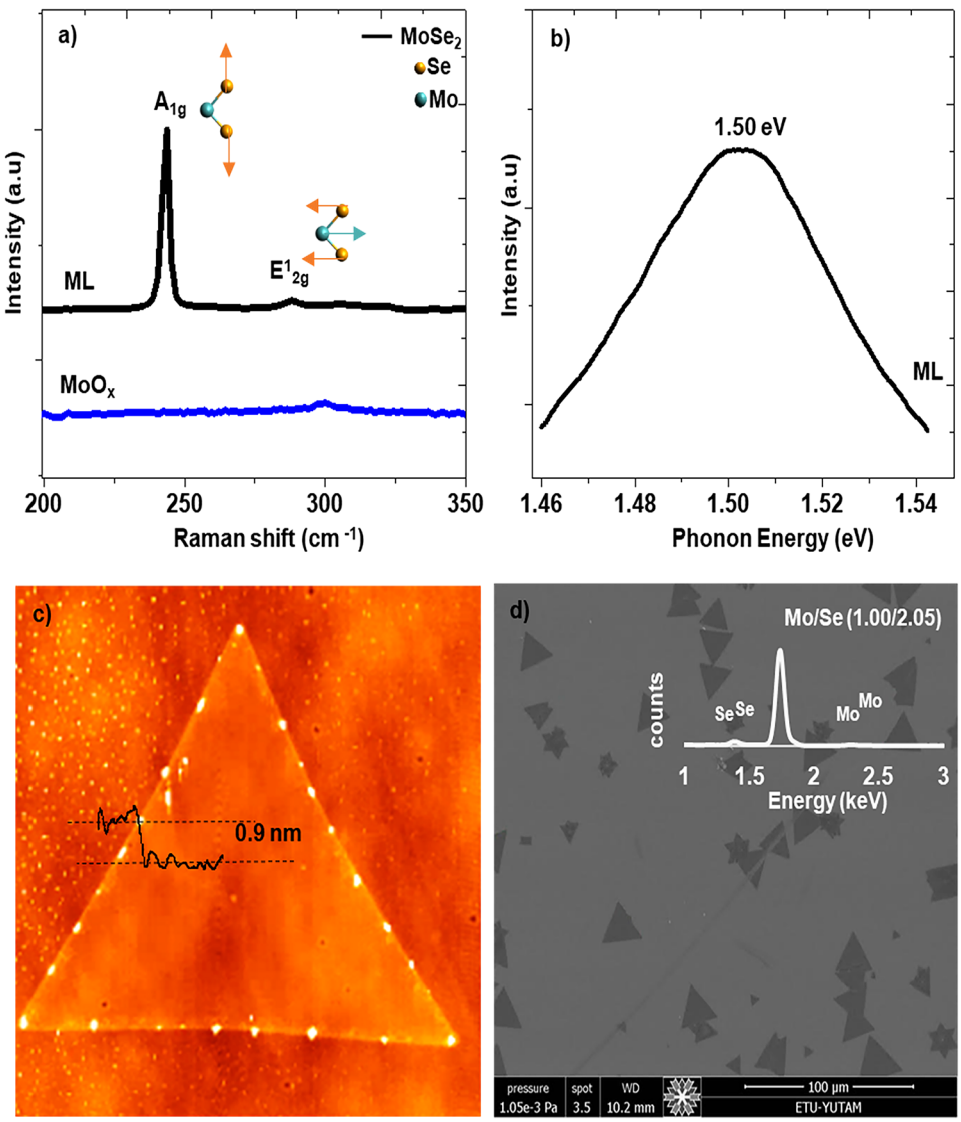

Fig. 2 **a** Raman spectrum of synthesized monolayer $MoSe_2$ flakes and MoO_x. **b** PL spectrum of synthesized monolayer $MoSe_2$ flakes. **c** AFM pictures and flake height profiles. **d** SEM images and EDX spectra of $MoSe_2$ nanoflakes

quantity of powder is gradually raised from 2 mg to 4 mg, the transition toward the hexagonal form varies depending on the metal or chalcogen composition of the structure. The literature indicates that the shape of the flake structures formed is determined by the disparity in edge formation energy between Mo-edge and Se-edge termination. This discrepancy in edge formation energy, depending on Mo-edge or Se-edge termination, leads to the formation of triangular-shaped particles [25–27]. The study on MoS_2 found that whether the ratio of Mo or S precursors is larger than 1:2 (Mo terminated) or less (S terminated), the structure takes on a triangular shape. However, when the Mo:S ratio is 1:2, a hexagonal shape is seen [28]. It was seen that the erosion that occurs on the edges and inside of triangular structures in Fig. 1b and c can be resulted from the hydrogen [29] or oxygen [30] gases used during the experiment.

During the experiment, the introduction of H_2 gas into the tube at high temperatures serves as a reducing agent [31]. This is crucial for the formation of $MoSe_2$ monolayers and assures the reduction of the MoO_3 precursor to MoO_{3-x} [32]. Due to the low concentration of hydrogen, it can lead to the generation of by-products such as MoO_x instead of producing $MoSe_2$ using the metal oxide precursor. By increasing the hydrogen concentration, the oxygen ions react with hydrogen to create water molecules, thereby inhibiting the production of hydrogen intermediates or by-products. Consequently, this reduces the probability of forming MoO_x [33]. Nevertheless, small amounts of oxide layers may appear in blue spots either on the surface or at the edge on within yellow circles on Fig. 1d and some layer may be linked to the oxide form of Mo. But our Raman results did not show any crystal oxide residue of Mo showing the presence of potential amorphous structures.

By increasing the flow rate of H_2 gas from 3 sccm (Fig. 1b) to 5 sccm (Fig. 1e), the experiment demonstrated that hydrogen inhibited the formation of multiple layers on the surface [34], hence facilitating the synthesis of predominantly monolayer $MoSe_2$. Experiments performed in the absence of hydrogen have shown that the inclusion of hydrogen decreases the number of layers, but it may also lead to a modest reduction in the lateral size. This is analogous to previous research in which the size of the domain diminishes in the presence of hydrogen [35, 36]. When the hydrogen is increased to 7 sccm (as shown in Fig. 1g) during synthesis, its flow rate in the tube will be greater compared to 1 sccm of H_2. Higher flow rates lead to a proportional rise in pressure. According to the theory of two-dimensional nucleation, higher pressures correspond to greater rates of nucleation. As the pressure rises, the number of individual atoms that adhere to the surface likewise increases, leading to an increase in nucleation [25].

Nanofabricated materials are mostly cleaned by organic solvents including acetone and IPA which may influence the PL emission and Raman properties of TMDCs. Therefore, Raman and PL measurements were retaken 10 min after acetone and IPA droplets were placed on the $MoSe_2$ monolayer. In Fig. 3b, it can be seen that there is no peak shifting for A_{1g} with acetone or IPA. However, E_{2g} mode slightly shifts (1.2 cm^{-1}) to high wavenumbers. PL spectra are also recollected after acetone and IPA treatments and it shows there is about 80-meV blue shift for all processes (see Fig. 4). Another striking process can be seen for PL peak intensities. For acetone treatment, the PL peak increases three times and non-radiative recombination

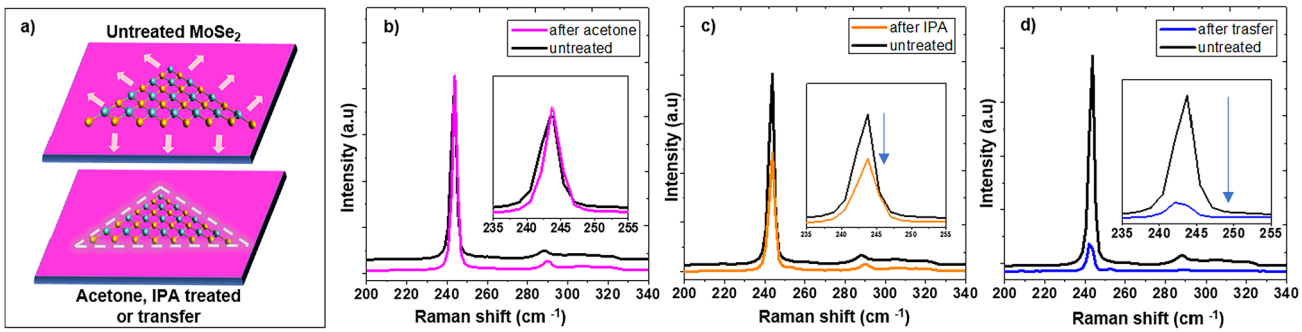

Fig. 3 **a** Schematic illustration of strain relaxation of $MoSe_2$. **b**, **c,** and **d** Raman spectra of $MoSe_2$ monolayers after acetone, IPA treatments, and PMMA transfer

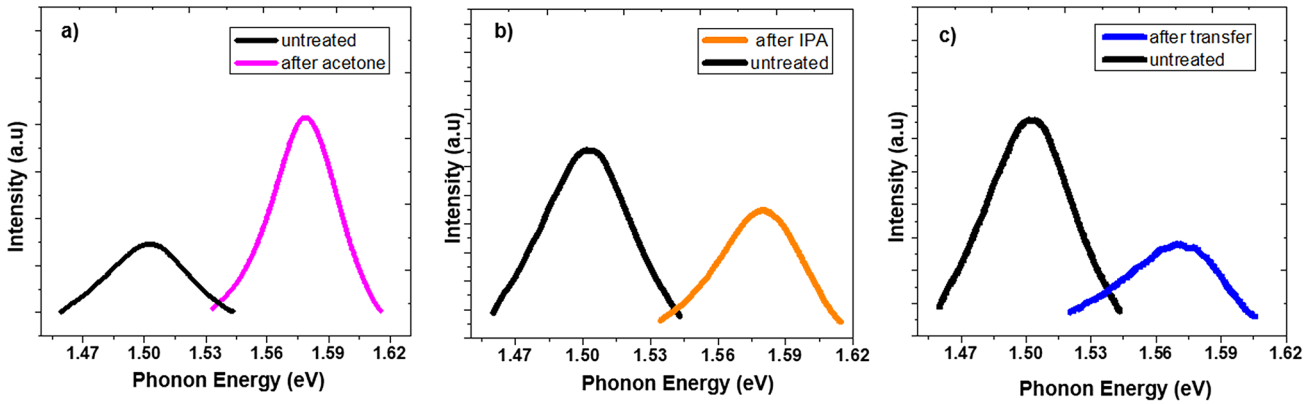

Fig. 4 PL spectra of $MoSe_2$ monolayers after treatnents of **a** acetone, **b** IPA, and **c** PMMA transfer

decreases. However, IPA treatment causes a decrease in the PL peak intensity. These variations can be explained as follows: (i) For monolayer TMDC materials, the excitons have been confined to the single-layer plane and they experienced small screening owing to the small dielectric environment and the tightly bounded excitons form due to strong coulombic interaction [37, 38]. In an experimental study conducted by Lin et al. [39], the PL and Raman measurements were taken in the different mediums, such as ethanol, acetone, IPA, methanol, hexanes, benzene, and 2-butanone, to show the effect of dielectric environment on exciton and trion PL peaks of MoS_2. They indicated that a blue shift up to 40 meV of exciton or trion PL peaks and PL intensity enhancement were observed with high dielectric constant of environment based on dielectric screening effect. According to this approach, we should expect an enhancement in the PL intensity and blue shift for both acetone and IPA due to their high dielectric constants [39]. Moreover, we can expect a change in the Raman peaks for this view. However, we observed only a small shift in in-plane Raman peak for acetone and IPA treatments and a decrease in the PL and Raman peaks for IPA treatment. Since we consider that the solvents are completely evaporated before PL and Raman measurements, this approach may not be considered appropriate to explain PL and Raman variations. (ii) The second effect can be doping for monolayer TMDC materials. In the literature, p-type doping is found to be the most general chemical treatment mechanism for n-type $MoSe_2$, MoS_2, and WS_2 materials [20, 40]. For these materials, the trion emission is at low energies with lower emission efficiency than neutral excitons and p-type doping dominates the emission of neutral excitons over trions, which leads to enhancement PL intensity and blue shift of PL peak position [41, 42]. Han et al. [20] indicated that the HBr treatment, which is p-type doping, led to an enhancement in the PL intensity of $MoSe_2$, an intensity increment, and an upshift in the out-of-plane Raman peak (phonon hardening). According to the study conducted by Choi et al. [43], it is obvious that both acetone and IPA will give electron to the $MoSe_2$, which is n-type doping, and this may explain the decrease in the PL peak and the Raman decrease in A_{1g} for IPA treatment due to expecting the opposite behavior in the PL and Raman peaks with n-type doping. But we cannot explain the effect of acetone treatment on the PL and Raman spectra based on the doping model. (iii) The last effect is definitely the strain to explain acetone and IPA treatments. The shift of in-plane Raman mode can be related to in-plane tensile strain releasing for $MoSe_2$, which is in good harmony with earlier studies [10, 12]. We can prove this with PMMA-transferred $MoSe_2$ on sapphire with same shifting. From Fig. 2a, acetone treatment cannot cause any damage to $MoSe_2$ because of no-changing Raman peak intensities. The Raman peak intensities for IPA treatment and transferred $MoSe_2$ samples decrease due to permanent damage to $MoSe_2$. It can be concluded that high vapor pressure of acetone accelerated the relaxation of surface tension between the decoupled $MoSe_2$ monolayer and substrate with less/no damage on $MoSe_2$ compared to IPA. The blue shift in the PL spectra clearly shows that $MoSe_2$ have a strong interaction with SiO_2. As the exciton binding energy in TMDC is expected to be nearly independent of the uniaxial strain, the energy shift of the PL emission can be directly correlated with reduction of band gap in the monolayer

flakes [23]. The band gap value after strain releasing is pretty harmony with the values of unstrained $MoSe_2$ single layers [13], which reveals that the completely releasing of strain. The similar blue shift (80 meV) was observed for CVD-grown WSe_2 monolayer after treatment and transfer [16], but it was observed that this shift was not stable in a study conducted by Chen et al. [17], which varied from 2 meV to 54 meV for MoS_2 and $MoSe_2$. When acetone and IPA vaporize from $MoSe_2/SiO_2$, the surface tension due to acetone and IPA draws the $MoSe_2$ from the substrate and breaks the strong interaction between $MoSe_2$ and SiO_2. This indicates that the surface tension values of acetone (24.5 mN/m) and IPA (23.0 mN/m) are higher than the interaction between $MoSe_2$ and SiO_2. The strain releasing can also be approved with Raman results that explained above. In the literature, the theoretical and experimental studies indicated that strain causes the band gap to decrease and direct to indirect band transition [10–12, 44, 45]; therefore, PL band position shifts to red with strain. For PL peak intensities, acetone treatment leads to the PL peak which increases three times and non-radiative recombination decreases which is clearly related to strain decoupling [16, 17]. However, IPA treatment and PMMA transfer process cause a decrease in the PL peak intensity. This can be related to structural damages after harsh chemicals, which is in good harmony with Raman results.

4 Conclusion

In the present work, it achieved a PL enhancement for CVD-grown $MoSe_2$ monolayers. The strong interaction between grown material and substrate led to strain, which resulted in decreasing PL intensity. Here, we showed when the interaction was broken with acetone and IPA, the emission peak shifted to blue and PL intensity enhanced about three times. It was seen that acetone had no damaging effect on $MoSe_2$ sample. When we compared the results with transferred $MoSe_2$, it was seen that the PL intensity drastically decreases after transfer due to harsh transferring process. The results reveal that CVD-grown $MoSe_2$ samples can be easily implemented to any optoelectronic application after acetone treatment.

Author contributions

ASK and AC have equal contributions to the study. GT designed the whole experiments. ASK and AC performed the sample synthesis and measurements. GT, ASK, AC, MAÇ and ME analyzed the results.

Funding

Open access funding provided by the Scientific and Technological Research Council of Türkiye (TÜBİTAK). G.T. acknowledges the financial support from The Scientific and Technological Research Council of Turkey (TÜBİTAK) (grant numbers: 120F234, 122F023, and 123F332).

Data availability

Datasets generated during the current study are available from the corresponding author on reasonable request.

Declarations

Conflict of interest The authors affirm that they do not have any known competing financial interests or personal relationships that could have influenced the work presented in this paper.

Open Access This article is licensed under a Creative Commons Attribution 4.0 International License, which permits use, sharing, adaptation, distribution and reproduction in any medium or format, as long as you give appropriate credit to the original author(s) and the source, provide a link to the Creative Commons licence, and indicate if changes were made. The images or other third party material in this article are included in the article's Creative Commons licence, unless indicated otherwise in a credit line to the material. If material is not included in the article's Creative Commons licence and your intended use is not permitted by statutory regulation or exceeds the permitted use, you will need to obtain permission directly from the copyright holder. To view a copy of this licence, visit http://creativecommons.org/licenses/by/4.0/.

References

1. A.K. Geim, K.S. Novoselov, Nat. Mater. **6**, 183 (2007)
2. K.F. Mak, C. Lee, J. Hone, J. Shan, T.F. Heinz, Phys. Rev. Lett. **105**, 2–5 (2010)
3. A. Splendiani, L. Sun, Y. Zhang, T. Li, J. Kim, C.-Y. Chim, G. Galli, F. Wang, Nano Lett. **10**, 1271–1275 (2010)
4. M. Saadati, O. Akhavan, H. Fazli, S. Nemati, H. Baharvand, ACS Appl. Mater. Interfaces. **15**, 3713–3730 (2023)
5. S. Hu, Q. Jiang, S. Ding, Y. Liu, Z. Wu, Z. Huang, T. Zhou, Z. Guo, J. Hu, ACS Appl. Mater. Interfaces. **10**, 25483–25492 (2018)
6. D. Mayes, F. Farahmand, M. Grossnickle, M. Lohmann, M. Aldosary, J. Li, V. Aji, J. Shi, J.C.W. Song, N.M. Gabor, PNAS (2023). https://doi.org/10.1073/pnas.2221815120
7. Y.-H. Chang, W. Zhang, Y. Zhu, Y. Han, J. Pu, J.-K. Chang, W.-T. Hsu, J.-K. Huang, C.-L. Hsu, M.-H. Chiu, T. Takenobu, H. Ji, C. Wu, W.-H. Chang, A. Thye, S. Wee, L.-J. Li, ACS Nano. **8**, 8582–8590 (2014)
8. X. Tian, R. Wei, S. Liu, Y. Zhang, J. Qiu, Nanoscale. **10**, 752 (2018)
9. H.-V. Han, A.-Y. Lu, L.-S. Lu, J.-K. Huang, H. Li, C.-L. Hsu, Y.-C. Lin, M.-H. Chiu, K. Suenaga, C.-W. Chu, H.-C. Kuo, W.-H. Chang, L.-J. Li, Y. Si, ACS Nano. **10**, 1454–1461 (2016)
10. C.R. Zhu, G. Wang, B.L. Liu, X. Marie, X.F. Qiao, X. Zhang, X.X. Wu, H. Fan, P.H. Tan, T. Amand, B. Urbaszek, Phys. Rev. B **88**, 121301(R) (2013)
11. H.J. Conly, B. Wang, J.I. Zieger, R.F. Jr. Haglumd, S.T. Pantelides, K.I. Bolotin, Nano Lett. **13**, 3626–3630 (2013)
12. Z. Liu, M. Amani, S. Najmaei, Q. Xu, X. Zou, W. Zhou, T. Yu, C. Qiu, A.G. Birdwell, F.J. Crowne, R. Vajtai, B.I. Yakobson, Z. Xia, M. Dubey, P.M. Ajayan, J. Lou, Nat. Commun. **5**, 5246 (2014)
13. X. Cheng, L. Jiang, Y. Li, H. Zhang, C. Hu, S. Xie, M. Liu, Z. Qi, Appl. Surf. Sci. **521**, 146398 (2020)
14. H. Wang, D. Zhu, F. Jiang, P. Zhao, H. Wang, Z. Zhang, X. Chen, C. Jin, Nanotechnology. **29**(9), 314001 (2018)
15. B. Peng, H. Zhang, H. Shao, Y. Xu, X. Zhang, H. Zhu, RSC Adv. **6**, 5767–5773 (2016)
16. H. Kim, G.H. Ahn, J. Cho, M. Amani, J.P. Mastandrea, C.K. Groschner, D.-H. Lien, Y. Zhao, J.W. Ager, M.C. Scott, D.C. Chrzan, A. Javey, Sci. Adv. **5**, eaau4728 (2019)
17. K. Chen, S. Deng, E. Chen, S. Wen, T. Ouyang, X. Wang, R. Zhan, J. Cai, X. Wan, H. Chen, ACS Appl. Mater. Interfaces. **13**, 44814–44823 (2021)
18. B.R. Borodin, F.A. Benimetskiy, V.Y. Davydov, A.N. Smirnov, I.A. Eliseyev, P.A. Alekseev, 2D Mater. **9**, 015010 (2021)
19. A.O.A. Tanoh, J. Alexander-Webber, Y. Fan, N. Gauriot, J. Xiao, R. Pandya, Z. Li, S. Hofmann, A. Rao, Nanoscale Adv. **3**, 4216–4225 (2021)
20. H.-V. Han, A.-Y. Lu, L.-S. Lu, J.-K. Huang, H. Li, C.-L. Hsu, Y.-C. Lin, M.-H. Chiu, K. Suenaga, C.-W. Chu, H.-C. Kuo, W.-H. Chang, L.-J. Li, Y. Shi, ACS Nano. **10**, 1454–1461 (2016)
21. S. Mouri, Y. Miyauchi, K. Matsuda, Nano Lett. **13**, 5944–5948 (2013)
22. M. Mahjouri-Samani, L. Liang, A. Oyedele, Y.-S. Kim, M. Tian, N. Cross, K. Wang, M.-W. Lin, A. Boulesbaa, C.M. Rouleau, A.A. Puretzky, K. Xiao, M. Yoon, G. Eres, G. Duscher, B.G. Sumpter, D.B. Geohegan, Nano Lett. **16**, 5213–5220 (2016)
23. J.O. Island, A. Kuc, E.H. Diependaal, R. Bratschitsch, H.S.J. van der Zant, T. Heine, A. Castellanos-Gomez, Nanoscale **8**, 2589 (2016)
24. M. Saadati, O. Akhavan, Catalysts. **11**, 1445 (2021)
25. C. Jung, S.M. Kim, H. Moon, G. Han, J. Kwon, Y.K. Hong, I. Omkaram, Y. Yoon, S. Kim, J. Park, Sci. Rep. **5**, 1 (2015)
26. Y. Jung, E. Ji, A. Capasso, G.-H. Lee, Y. Jung, E. Ji, A. Capasso, G.-H. Lee, J. Korean Ceram. Soc. **56**, 24 (2019)
27. N. Masurkar, N.K. Thangavel, L.M.R. Arava, ACS Appl. Mater. Interfaces. **10**, 27771 (2018)
28. S. Wang, Y. Rong, Y. Fan, M. Pacios, H. Bhaskaran, K. He, J.H. Warner, Chem. Mater. **26**, 6371 (2014)
29. Y. Hwang, S.G. Kang, N. Shin, ACS Appl. Mater. Interfaces. **12**, 34297 (2020)
30. J. Li, S. Hu, Z. Chen, Y. Liang, H. Kang, Y. Zhang, Y. Sui, S. Wang, G. Yu, S. Peng, Z. Jin, X. Liu, Appl. Surf. Sci. **510**, 145412 (2020)
31. J. Chen, X. Zhao, S.J.R. Tan, H. Xu, B. Wu, B. Liu, D. Fu, W. Fu, D. Geng, Y. Liu, W. Liu, W. Tang, L. Li, W. Zhou, T.C. Sum, K.P. Loh, J. Am. Chem. Soc. **139**, 1073 (2017)
32. C. González, J.P.B. Silva, A.S. Viana, K. Gwozdz, O. Conde, Appl. Surf. Sci. **605**, 154742 (2022)
33. H. Wang, D. Zhu, F. Jiang, P. Zhao, H. Wang, Z. Zhang, X. Chen, C. Jin, Nanotechnology. **29**, 314001 (2018)
34. H.G. Ji, Y.C. Lin, K. Nagashio, M. Maruyama, P. Solís-Fernández, A. Sukma, V. Aji, S. Panchal, K. Okada, Suenaga, H. Ago, Chem. Mater. **30**, 403 (2018)
35. Y. Sheng, H. Tan, X. Wang, J.H. Warner, Chem. Mater. **29**, 4904 (2017)
36. S. Hong, C.K. Rhee, Y. Sohn, Catalysts. **96**(6), 494 (2019)
37. Y. You, X.-X. Zhang, T.C. Berkelbach, M.S. Hybertsen, D.R. Reichman, T.F. Heinz, Nat. Phys. **11**, 477–481 (2015)
38. M.M. Ugeda, A.J. Bradley, S.-F. Shi, F.H. da Jornada, Y. Zhang, D.Y. Qiu, W. Ruan, S.-K. Mo, Z. Hussain, Z.-X. Shen, F. Wang, S.G. Louie, M.F. Crommie, Nat. Mater. **13**, 1091–1095 (2014)

39. Y. Lin, X. Ling, L. Yu, S. Huang, A.L. Hsu, Y.-H. Lee, J. Kong, M.S. Dresselhaus, T. Palacios, Nano Lett. **14**, 5569–5576 (2014)
40. A. Wang, R. Tan, C. Breakwell, X. Wei, Z. Fan, C. Ye, R. Malpass-Evans, T. Liu, M.A. Zwijnenburg, K.E. Jelfs, N.B. McKeown, J. Chen, Q. Song, J. Am. Chem. Soc. **144**(37), 17198–17208 (2022)
41. N. Peimyoo, W. Yang, J. Shang, X. Shen, Y. Wang, T. Yu, ACS Nano. **8**, 11, 11320–11329 (2014)
42. H. Nan, Z. Wang, W. Wang, Z. Liang, Y. Lu, Q. Chen, D. He, P. Tan, F. Miao, X. Wang, J. Wang, Z. Ni, ACS Nano. **8**, 6, 5738–5745 (2014)
43. J. Choi, H. Zhang, H. Du, J.H. Choi, ACS Appl. Mater. Interfaces. **8**, 14, 8864–8869 (2016)
44. M. Buscema, G.A. Steele, H.S.J. van der Zant, Nano Res. **7**, 561 (2014)
45. N. Scheuschner, O. Ochedowski, A.-M. Kaulitz, R. Gillen, M. Schleberger, J. Maultzsch, Phys. Rev. B **89**, 125406 (2014)

Publisher's Note Springer nature remains neutral with regard to jurisdictional claims in published maps and institutional affiliations.